UC Davis
San Francisco Estuary and Watershed Science

Title

Dispersion Mechanisms of a Tidal River Junction in the Sacramento–San Joaquin Delta, California

Permalink

Journal

Authors

Gleichauf, Karla T.
Wolfram, Phillip J.
Monsen, Nancy E.
et al.

Publication Date

2014

DOI

Copyright Information

Peer reviewed

SAN FRANCISCO
ESTUARY & WATERSHED SCIENCE
Sponsored by the Delta Science Program and the UC Davis John Muir Institute of the Environment

Dispersion Mechanisms of a Tidal River Junction in the Sacramento–San Joaquin Delta, California

Karla T. Gleichauf*[1], Phillip J. Wolfram[1,2], Nancy E. Monsen[1], Oliver B. Fringer[1], and Stephen G. Monismith[1]

ABSTRACT

In branching channel networks, such as in the Sacramento–San Joaquin River Delta, junction flow dynamics contribute to dispersion of ecologically important entities such as fish, pollutants, nutrients, salt, sediment, and phytoplankton. Flow transport through a junction largely arises from velocity phasing in the form of divergent flow between junction channels for a portion of the tidal cycle. Field observations in the Georgiana Slough junction, which is composed of the North and South Mokelumne rivers, Georgiana Slough, and the Mokelumne River, show that flow phasing differences between these rivers arise from operational, riverine, and tidal forcing. A combination of Acoustic Doppler Current Profile (ADCP) boat transecting and moored ADCPs over a spring–neap tidal cycle (May to June 2012) monitored the variability of spatial and temporal velocity, respectively. Two complementary drifter studies enabled assessment of local transport through the junction to identify small-scale intrajunction dynamics. We supplemented field results with numerical simulations using the SUNTANS model to demonstrate the importance of phasing offsets for junction transport and dispersion. Different phasing of inflows to the junction resulted in scalar patchiness that is characteristic of MacVean and Stacey's (2011) advective tidal trapping. Furthermore, we observed small-scale junction flow features including a recirculation zone and shear layer, which play an important role in intra-junction mixing over time scales shorter than the tidal cycle (i.e., super-tidal time scales). The study period spanned open- and closed-gate operations at the Delta Cross Channel. Synthesis of field observations and modeling efforts suggest that management operations related to the Delta Cross Channel can strongly affect transport in the Delta by modifying the relative contributions of tidal and riverine flows, thereby changing the junction flow phasing.

KEYWORDS

Junction dispersion, flow phasing, tidal trapping, super-tidal time scales, Delta Cross Channel

INTRODUCTION

Hydrodynamic processes in the Sacramento–San Joaquin River Delta affect ecosystem function through the transport of salt, sediments, heat, contaminants including selenium and ammonium, and,

in more complex ways involving behavior, organisms such as larval fish. In turn, spatial and temporal variability of key physical variables—e.g., water temperature and salinity—help determine suitability of the diverse Delta environments for native species such as the Delta Smelt and Chinook salmon (Feyrer et al. 2010). In general, the distribution of these scalars is determined by a balance of subtidal advection and dispersion arising from tidal averaging (Fischer et al. 1979; Denton 1993; Monismith et al. 2009). Bulk dispersion in the Delta results from mixing that occurs at both local and system-wide scales (Kimmerer and Nobriga 2008) through pathways involving single and multiple junctions.

Monismith et al. (2009) found that the San Joaquin along-channel subtidal dispersion coefficient was $K \sim 1000 \ m^2 s^{-1}$, which is one order of magnitude larger than the typical value of $K \sim 100 \ m^2 s^{-1}$ inferred from the observed the along-channel temperature gradient. Drawing on the analogous case of chaotic dispersion described by Ridderinkhof and Zimmerman (1992), Monismith et al. (2009) attributed this behavior to the dispersive effects of flows through the many junctions of the Delta, implying that flow characteristics at channel junctions may substantially change transport patterns in the Delta. From a modeling perspective, this suggests that if junction dynamics are not resolved, as is the case for the DSM2 Particle Tracking Model (Kimmerer and Nobriga 2008), modeled dispersion may differ from the actual mixing processes that occur at junctions. For example, DSM2 Particle Tracking assumes that particles at a junction are instantaneously and completely mixed, distributing particles out of the junction based on the fractional volume outflow. However, junction dynamics such as recirculation zones, shear layers, and phasing may distribute those particles differently. Furthermore, DSM2 resolves the tides, whereas other transport models may use tidally averaged flows. In both tidal and tidally averaged one-dimensional models, longitudinal dispersion coefficients are needed to account for tidal and super-tidal processes, i.e. time scales smaller than a tidal cycle. Thus, better representation of longitudinal dispersion at Delta junctions that account for complex physics within junctions should improve the predictive ability of less resolved hydrodynamic models.

A priori estimates of mixing in Delta channels can be made by computing longitudinal dispersion coefficients from well-known formulae given in the estuarine literature (e.g., Okubo 1973; Fischer et al. 1979; Geyer and Signell 1992) that are generally based on the Taylor (1954) shear flow dispersion mechanism. More recently, MacVean and Stacey (2011) related advective tidal trapping at a tidal slough to enhanced dispersion. Like Okubo's (1973) diffusive trapping, these dispersion estimates arise from temporally lagged storage in channels or embayments connected to the main channel. However, MacVean and Stacey (2011) assume the dominant mixing processes result from temporal lags caused by advective processes. The role of advective trapping at junctions has previously been unexplored. Our analysis of principal mixing processes that occur in Delta junctions extends understanding of junction dispersion as well as tidal trapping.

We present results of field observations and hydrodynamic modeling designed to examine in detail the behavior of flows and mixing at a Delta junction. We will show that tidal river junction dynamics affect dispersion in a fashion similar to that described by MacVean and Stacey (2011), in that water masses are separated because of phase differences in junction inflows and outflows. The phase differences result from tidal modification of the riverine inflows over different time scales and magnitudes. We also demonstrate that junction flow features such as separation zones and shear layers contribute to mixing in the junction on super-tidal time scales.

Site Description

Georgiana Slough junction (GSJ) is an ideal site to consider junction dispersion because of its geometry, size, relative simplicity of inflows and outflows, and its location downstream of the Delta Cross Channel (DCC) (Figure 1). The DCC is a 1,830-m long diversion channel that routes up to 100 $m^3 s^{-1}$ (3,500 cfs) of water from the Sacramento River at Walnut Grove into a stem of the Mokelumne River (USBR 2013). The DCC helps maintain water quality in the Delta by reducing saltwater intrusion and providing water with fewer agricultural pollutants and contaminants
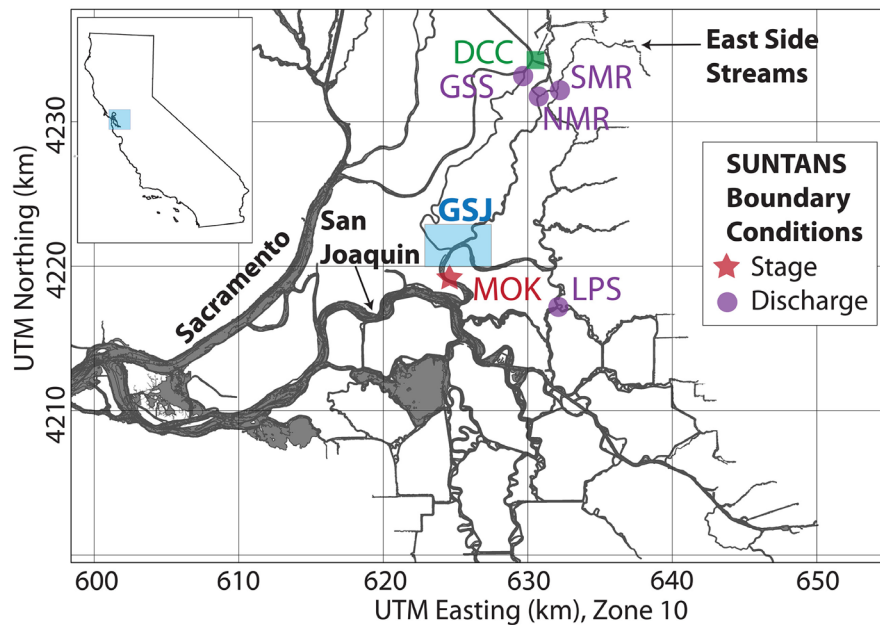
Figure 1 The Sacramento–San Joaquin River Delta with the simulation domain and the junction study site, Georgiana Slough junction (GSJ**)**, highlighted by the blue rectangle. The Delta Cross Channel (DCC; USGS #11336600) is indicated by the green box.

to the Delta. Opening the gates directs water from the Sacramento River to the Mokelumne River for 15 miles to the San Joaquin and eventually, after 35 miles, through Old and Middle rivers to the state and federal pumping plant intakes. This water is then routed to the Central Valley and southern California (USBR 2013). While the DCC gates open to enhance water quality in the interior Delta, the gates close for flood protection when the Sacramento River flows are too high, and to discourage Chinook salmon from migrating into the central Delta. The gates are typically closed from February 1 through May 15 and intermittently until June 15, as well as periods in between October 1 and January 31, depending on the timing of the fish migration.

DCC operations greatly affect dispersion at GSJ since three of its branches, namely Georgiana Slough and the North and South Mokelumne rivers, are directly downstream of the DCC (Figures 1 and 2A). The fourth branch of GSJ is the Mokelumne River, which is approximately 5 km north of the San Joaquin River. The main channel in the junction that connects all four branches is approximately 950-m long (Figure 2B). The width of Georgiana Slough (GS) is

70 m, the Mokelumne (MOK) is 160 m, the middle of the junction is 265 m, the North Mokelumne (NMK) is 140 m, and the South Mokelumne (SMK) is 175 m. GSJ consists of two confluence or diffluence junctions, depending on the tidal phase, connected by a main channel. A confluence is composed of two channels meeting whereas a diffluence is composed of one channel branching into two. The GS and MOK confluence/diffluence will be referred to as the west junction, the confluence/diffluence of NMK and SMK the east junction, and the channel connecting them as the main channel (Figure 2B).

GS and NMK serve as the primary riverine inflows and MOK and SMK as the estuary source water inflows (Figure 2B). The junction is forced by tidal flows originating from the west that propagate up from San Francisco Bay through the San Joaquin River and into the southern rivers of MOK and SMK (Figure 1 and 2B). In addition to the tides, GSJ flow is forced by three rivers. Most of the freshwater input to GSJ is derived from the Sacramento River, which is heavily influenced by gate operations at the DCC; the Mokelumne and Cosumnes rivers contribute small amounts of freshwater flow to the junction (Figure 1).
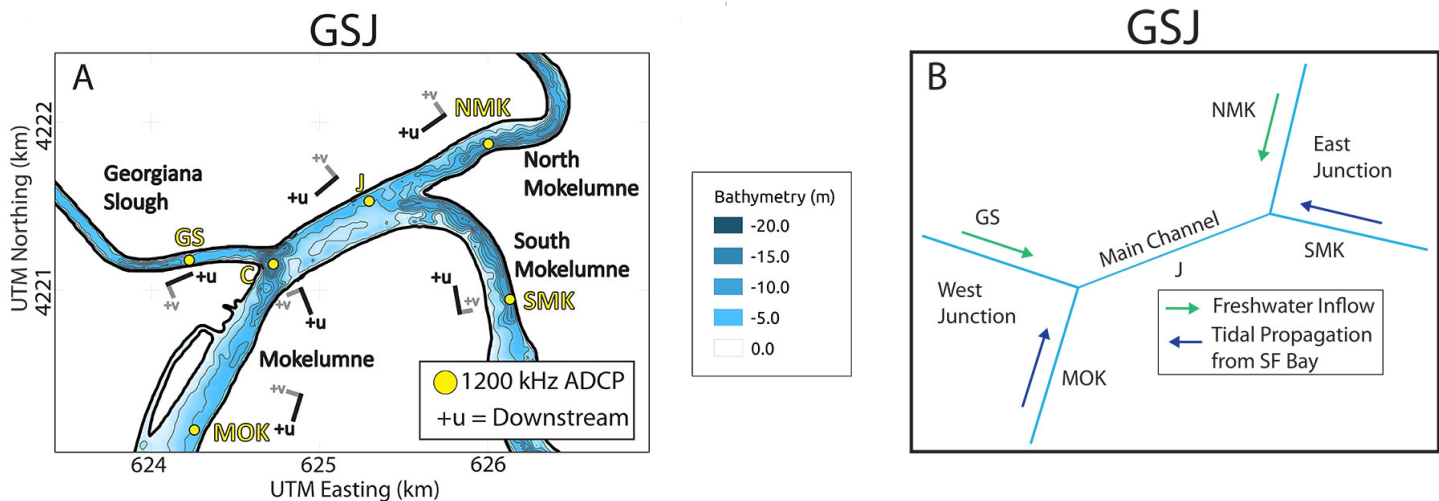
Figure 2 (A) Detail of the Georgiana Slough junction (GSJ) experimental design. Yellow dots represent the 1200-kHz ADCPs that were moored from May 31 through June 19, 2012. Positive alongshore (+u) and cross shore (+v) velocities are shown with black and grey lines. The positive alongshore velocity points downstream, generally in the ebb tide direction, and is given by the semi-major axis of the tidal ellipse. **(B)** Conceptual model of Sacramento freshwater (green) and estuary source water from San Francisco (SF) Bay (dark blue) inflows to GSJ. The main channel connects the west junction, composed of GS and MOK, to the east junction, composed of NMK and SMK.

When the DCC is closed, only Georgiana Slough can carry Sacramento River-derived water to GSJ via the west junction. Opening the DCC routes Sacramento-derived water through both the NMK and GS to the GSJ (Figure 3).

Conditions During the Study Period

The study occurred from May 30 through June 19, 2012, a dry water year by the California Department of Water Resources (CDWR) classification. According to DAYFLOW estimates (*http://www.water.ca.gov/day-flow/*), the average outflow over the study period at the Sacramento, San Joaquin, and east side streams (Mokelumne and Cosumnes rivers) were 337, 46, and 56 $m^3 s^{-1}$, respectively, and 410 $m^3 s^{-1}$ for the entire Delta (Figure 1 for locations). The USGS flows at the Sacramento at Freeport (USGS #11447650; north of map in Figure 1), the San Joaquin at Vernalis (USGS #11303500; south of map in Figure 1), and the Delta Cross Channel (DCC) (USGS #11336600) are displayed in Figure 4.

The study period spanned times during which the DCC was both open (until June 4, 2012, at 17:00) and closed. The DCC is typically closed after Memorial

Day, May 28 in 2012, to encourage salmon migration in the Sacramento River. However, because of a mechanical failure, the gate was closed later providing an unplanned, unique opportunity to examine its effect on junction dynamics during the study.

METHODS

Field Observations

Three different field methods were used to examine spatial and temporal velocity variability at GSJ: Acoustic Doppler Current Profiler (ADCP) transecting, *in-situ* ADCP instrumentation, and drifter studies.

ADCP Transecting

The first stage of the fieldwork used a boat-mounted 1200 KHz Teledyne RD Instruments (TRDI) ADCP to monitor the spatial and temporal variability of velocity in both the west and east junctions and the main channel at GSJ. The boat-mounted ADCP was used on May 30, 2012 to obtain transects across the four branches and within the junction for approximately 12 hours.
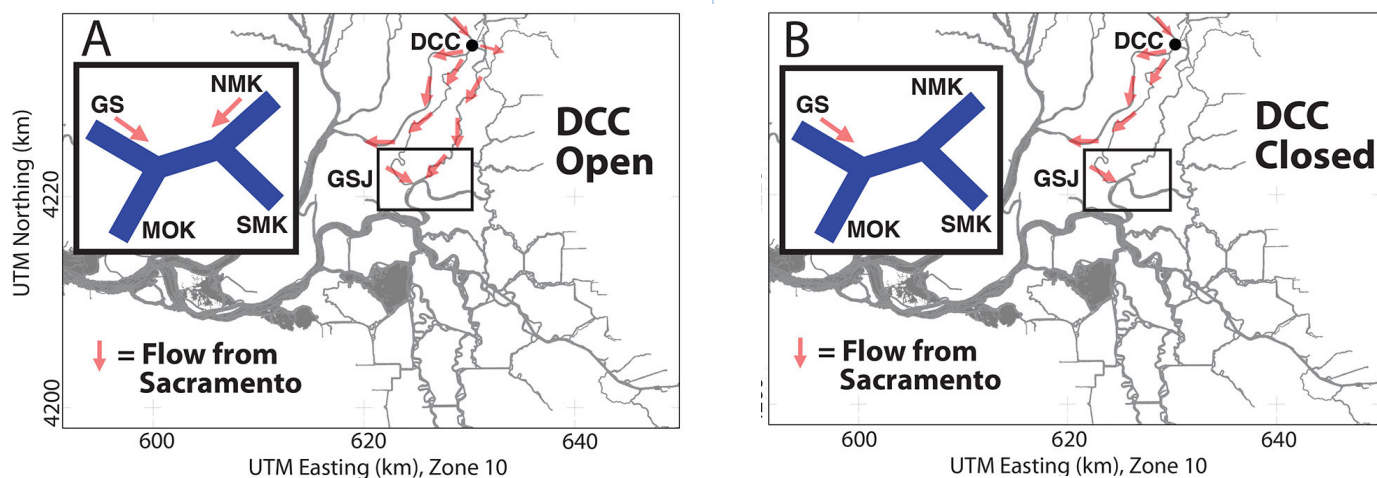
Figure 3 Movement of Sacramento River-derived water (in red arrows) to the central Delta when the DCC is open **(A)** vs. DCC closed **(B)**. The DCC was open at the beginning of the experiment and closed on June 4, 2012, at 17:00. The inset cartoon depicts the primary routes of Sacramento source water into GSJ.

In-Situ Instrumentation

Velocity and stage data were collected over a spring-neap tidal cycle from May 30 through June 19, 2012, where six 1200 kHz TRDI ADCPs were installed in the branches and within the junction (stations GS, C, J, NMK, SMK, MOK) (Figures 2A and 2B). The ADCPs took 1 Hz single ping 1 second data for 2.5 weeks with 25-cm resolution in the vertical.

Velocities were rotated into local along-channel (u) and cross-channel (v) components using principal axes analysis (Emery and Thomson 2004), with positive velocities defined as downstream flow (Figure 2A). In the GSJ and in much of the Delta where rivers and tides are interacting, velocities are not necessarily upstream during flood and downstream during ebb tides.

Since little vertical variability was observed in the water column at GSJ, the velocity data were depth-averaged and time-averaged using a 10-minute window. Because of high sediment loads obstructing ADCP measurements at three ADCP mooring stations, the Lomb–Scargle method, which is an unevenly spaced spectral interpolant technique, was applied to interpolate missing depth-averaged velocity data at
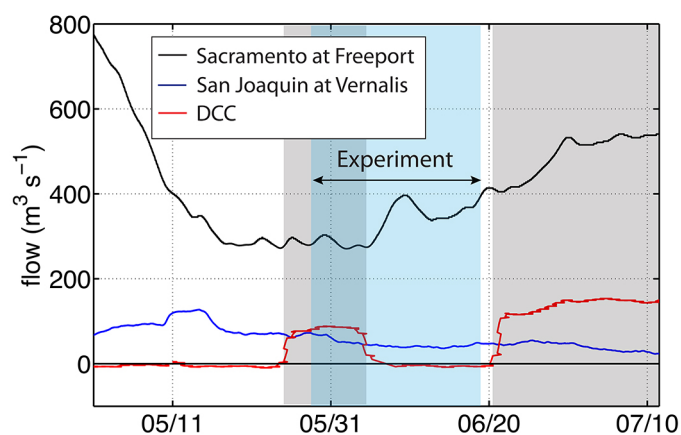

Figure 4 Flow at Sacramento at Freeport (USGS #11447650), San Joaquin at Vernalis (USGS #11303500), and DCC (USGS #11336600) from May 1 through July 11, 2012. The grey region highlights the period in which the Delta Cross Channel was open and the blue highlights the study period.

SMK (4% of data), NMK (2% of data), and J (11% of data), preserving the low-frequency components of the data set (Scargle 1982; Horne and Baliunas 1986).

Observed along-channel velocities were decomposed into tidal and subtidal (time-averaged) components. The subtidal along-channel velocity at the junction, $\langle u \rangle$, is defined to be the low-pass filtered velocity, obtained by taking a 25-hr, 4th-order, low-

pass Butterworth filter of the ADCP depth-averaged velocity. Note that the subtidal velocity is expected to reflect the subtidal effects of the various riverine inputs, although it can also include the rectified effects of the tides (Monsen 2000). The tidal component of the velocity, u_T, can be determined by subtracting the subtidal velocity $\langle u \rangle$ from the total velocity u:

$$u_T = u - \langle u \rangle \tag{1}$$

The subtidally varying strength of the tide is defined by computing the time-varying root mean square (rms) velocity u_{Trms}, which is the square root of the square of the low-pass filtered value of u_T

$$u_{Trms} = \sqrt{\left\langle u_T^2 \right\rangle} \tag{2}$$

The amount of tidal influence at the junction is examined using the power spectral density (PSD) of the velocity at each ADCP mooring (Emery and Thomson 2004), which displays the distribution of power per unit frequency. While system periodicities can often be extracted using harmonic analysis instead, harmonic analysis should not be applied to the interior of the Delta where strong modulations of tidal motions by gate operations and variations in river flow will likely interfere with the analysis (Monsen 2000). Harmonic analysis of signals in the inner Delta reveals that the low-pass, or subtidal, signals are not periodic. The behavior of the system is fundamentally altered because of the interaction of the mean flows and the associated water levels with the tides. In contrast, spectral analysis can extract tidal frequencies by calculating how the power of a signal varies with frequencies. In our case, the signal was the water velocity, and the frequencies containing the most power were the tidal frequencies. For this reason, the PSDs of the NMK and SMK velocities are computed for times when the DCC was open and closed to present the dominant frequencies during these periods.

Drifter Studies

To understand the motion of particles within the junction, Lagrangian drifters were released on

June 1 and June 8, 2012 when the DCC was open and closed, respectively. Fourteen Android phone surface drifters, built at the University of California at Berkeley for their Floating Sensor Project (*http://float.berkeley.edu*) (Tinka et al. 2013), and nine drifters with 1-m long water sails borrowed from the USGS California Water Science Center were deployed throughout the GSJ. Drifters were released in groups of 1 to 13 for deployments ranging from 1 to 9 hours and were typically retrieved when they drifted downstream or were trapped in dense vegetation. Table 1 highlights the details of the four drifter releases referenced in this paper.

The Android drifters can be monitored via a webpage and they are designed to follow the surface flow; hence, they can follow wind-driven surface currents. In contrast, the USGS drifters have 1 m water sails that track the mean flow better, and minimize the influence of the wind. However, the USGS drifters are difficult to monitor with a passive GPS and are frequently entangled in dense vegetation. While these differences in drifters were not ideal, the paths of the two types of drifters were similar, and the focus of this paper is to identify general mixing patterns in the junction rather than evaluate drifter models.

On June 1, 2012, 11 groups of drifters were released. Here we present the paths of drifter Groups 1 and 6 (Table 1), which highlighted the phase difference between NMK and SMK and lateral mixing when GS joined MOK flow, respectively. On June 8, 15 groups of drifters were deployed. Group 11 displays a type of tidal trapping in SMK and how a recirculation zone affected cross-sectional mixing and Group 12 shows the recirculation zone at MOK and GS. These four drifter groups demonstrate super-tidal flow features such as recirculation zones, shear layers, and mixing zones.

Hydrodynamic Modeling of the Experimental Period

To help interpret the field observations, we performed hydrodynamic modeling during the experimental period at GSJ using the unstructured-grid, open-source SUNTANS model (Fringer et al. 2006). The SUNTANS computational domain boundar-

Table 1 Details of selected drifter experiments on June 1, 2012 and June 8, 2012

Group #	1	6	11	12
Date Released	6/1/12	6/1/12	6/8/12	6/8/12
Feature represented	Phase lag between NMK and SMK	Cross-sectional mixing when GS joined MOK	Tidal trapping in SMK and transverse mixing from eddy at MOK/GS scour hole	Recirculation zone dynamics at the MOK/GS junction
Number of drifters	4	10	9	9
Release location	NMK	MOK	NMK (4); SMK (5)	GS
Pick-up location	SMK	SMK (5); J (3); MOK (2)	MOK (4); SMK (5)	MOK
DCC Configuration	Open	Open	Closed	Closed
Berkeley surface drifters or USGS sail drifters	2 surface; 2 sail	7 surface; 3 sail	6 surface; 3 sail	5 surface; 4 sail
Notes		Many retrieved in vegetation or under the bridge		3 retrieved from recirculation region

ies are shown in Figure 1. We used flow boundary conditions in the northern part of the domain for Georgiana Slough (GSS; USGS Station #11447903), the North Mokelumne River (NMR; USGS Station #11336685), the northern branch of the South Mokelumne River (SMR; USGS Station #11336680), and Little Potato Slough (LPS; USGS Station #11336790). We used a stage boundary condition at the southern part of the computational domain at the Mokelumne (MOK; USGS Station #11336930).

The unstructured, triangular grid contains a total of 127,265 grid cells in three-dimensions, with a mean horizontal grid resolution of approximately 8 m and a mean vertical resolution of 1.4 m. The grid resolution far from the junction is expanded to 40 to 50 m in the horizontal, while the vertical resolution is fixed at 1.4 m throughout the domain. A time step size of 1 second was used, giving a runtime of approximately five times real time on 8 Intel® Xeon® CPU X5550 at 2.67 GHz processors. The unstructured grid was generated with the Triangular Orthogonal Mesh (TOM) unstructured grid generation software (Holleman et al. 2013) and the bathymetry was from the USGS Foxgrover et al. (2003) data set.

Additionally, a constant drag coefficient of 0.003 was applied at the bottom.

The model was started from rest at 12:00 am on May 28, 2012 with a spin-up time of one-half day and was run until June 2, 2012 at 12:00 am. We introduced model tracers into the Georgiana Slough (red) and North Mokelumne (blue), respectively, to demonstrate the effect of flow phasing on scalar transport within the junction. All other inputs to the system were tracer-free. The model-derived tracer distributions highlight the movement and interactions of different water masses throughout the junction and are used to complement the field observations.

SUNTANS Validation for the GSJ Domain

We validated observed and predicted quantities with the Murphy and Epstein (1989) skill score (SS), which is the deviation of the RMS error normalized by the standard deviation of the observations from unity,

$$SS = 1 - \frac{\sum \left(X_{pred} - X_{obs} \right)^2}{\sum \left(X_{obs} - \overline{X_{obs}} \right)^2}$$

(3)

where X_{pred} is the predicted quantity, X_{obs} is the observed quantity, and $\overline{X_{obs}}$ is the temporal mean of the observed quantity at a particular spatial location. We assessed model performance with designations of excellent (SS > 0.65), very good (0.5 < SS < 0.65), good (0.2 < SS < 0.5), or poor (SS < 0.2) according to the classification scheme of Allen et al. (2007) and Marechal (2004). Skill scores were adopted for model validation to quantify relative model performance. In particular, we present the skill scores for depth-averaged flows since flows within the junction are typically vertically well-mixed because of the lack of stratification and overall low depth-to-width aspect ratio.

We compared model results to observations to assess model error, particularly for the ADCP mooring time series. Depth-averaged flow and system discharge were the primary determinants for model accuracy because junction dispersion is largely driven by flow phasing differences in channel inflows and outflows. Beyond these tidal-scale processes, the structure of super-tidal flow features is important in assessing their short time-scale effect on dispersion at the junction.

We consider model calibration to be very good because discharge and stage were well represented for flow in and out of the junction, depth-averaged streamwise flow agreed with ADCP observations, and larger-scale spatial structure of intrajunction flow features was obtained. The skill scores ranged from 0.85 to 0.98 with the exception of velocity at Georgiana Slough (SS = 0.61), where local bathymetry was not well represented in the model (Figure 5).

RESULTS

The results are divided into three sections based on ADCP, drifter, and modeling findings. First, the fixed ADCP station measurements display an Eulerian representation of the general circulation patterns bounding the junction with a focus on the larger Delta domain. In the second section, drifter data provides a Lagrangian view of the circulation patterns within GSJ and identifies key junction flow features needed to develop a conceptual model of how mixing occurs in this junction. Finally, we used the SUNTANS

hydrodynamic model to integrate and expand our conceptual junction model and to interpret the field results. Ultimately, the hydrodynamic model enabled analysis of spatial variability not readily apparent with the ADCP data, incorporating a broad and local view of the Delta and GSJ to further investigate how dispersion occurred in the junction.

ADCP Results

The fixed ADCP measurements elucidate that the GSJ circulation was dictated by the interplay of tides and riverine inflows. Each branch at GSJ experienced a different tidal and riverine influence, which was changed by the DCC operations.

Junction Circulation

The ADCP velocity time series shows that junction velocities varied between the bounds of +/− 0.5 m s^{-1} during ebb and flood tide and that most of the junction branches experienced asymmetric ebb and flood velocities (Figure 6). Also, both the east and west junctions were influenced by DCC operations. The stations with the largest velocity change, which were likely affected by the DCC closing, were GS (velocity minimum varying from −0.05 when the DCC was open to 0.2 m s^{-1} when closed in Figure 6A) and NMK (velocity minimum varying from −0.2 when open to −0.35 m s^{-1} when closed in Figure 6C), which is consistent with the general circulation pattern of Sacramento-derived water in the central Delta (Figure 3).

Subtidal Circulation

At each ADCP mooring, the mean velocities in the downstream and upstream directions were not necessarily equal in magnitude and changed once the DCC closed (Figure 6E). These flow changes can be attributed to the DCC's closure, which stopped Sacramento-derived water from flowing into the east junction (NMK) and routed more of it into the west junction via Georgiana Slough (GS). Since SMK mean flow changed little upon closing the DCC, mixing at SMK occurred predominantly from tides rather than
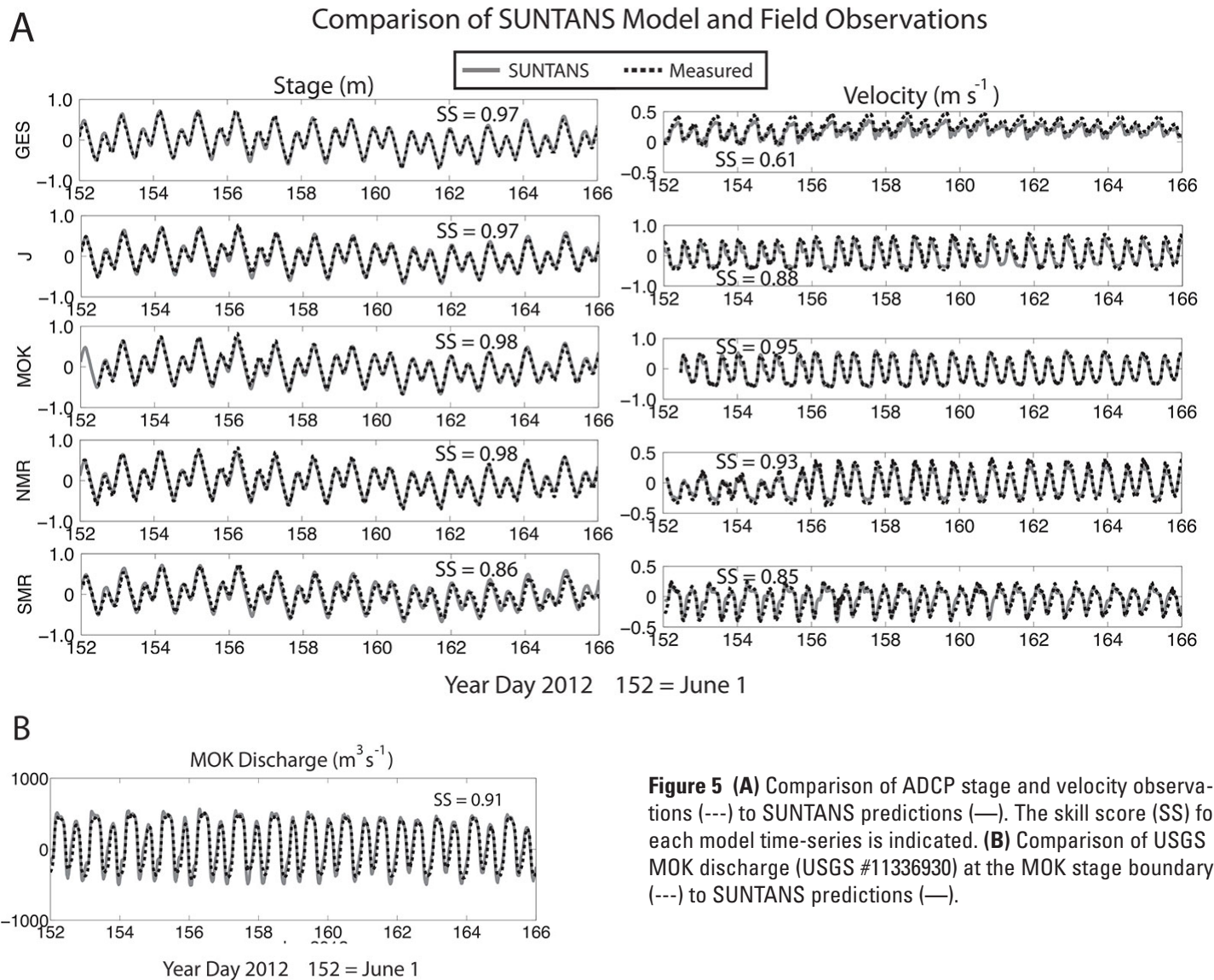
Comparison of SUNTANS Model and Field Observations

A

Stage (m) — **Velocity (m s⁻¹)**

GES: SS = 0.97, SS = 0.61
J: SS = 0.97, SS = 0.88
MOK: SS = 0.98, SS = 0.95
NMR: SS = 0.98, SS = 0.93
SMR: SS = 0.86, SS = 0.85

Year Day 2012   152 = June 1

B

MOK Discharge (m³ s⁻¹)

SS = 0.91

Year Day 2012   152 = June 1

Figure 5 (A) Comparison of ADCP stage and velocity observations (---) to SUNTANS predictions (—). The skill score (SS) for each model time-series is indicated. **(B)** Comparison of USGS MOK discharge (USGS #11336930) at the MOK stage boundary (---) to SUNTANS predictions (—).

river flow, regardless of gate operations during the experiment.

The subtidal velocities, representing riverine velocities, varied greatly within the junction. GS had the largest subtidal velocity magnitude, with a mean of $0.17\,\mathrm{m\,s^{-1}}$ when the DCC was open and $0.25\,\mathrm{m\,s^{-1}}$ when it was closed. In contrast, MOK, also in the west junction, had a negligible subtidal velocity throughout the entire time series. In the east junction, NMK had a subtidal velocity of $0.13\,\mathrm{m\,s^{-1}}$ when the DCC was open but decreased to nearly zero once the gates closed, while SMK subtidal velocity started at $0.07\,\mathrm{m\,s^{-1}}$ upstream when the DCC was open and decreased in magnitude to $0.05\,\mathrm{m\,s^{-1}}$ upstream (Figure 6D). These subtidal decompositions show that GS and NMK had mean velocities that flowed into the junction whereas SMK and, to a lesser extent, MOK flowed out of the junction.

Ratio of Subtidal to Tidal Velocity
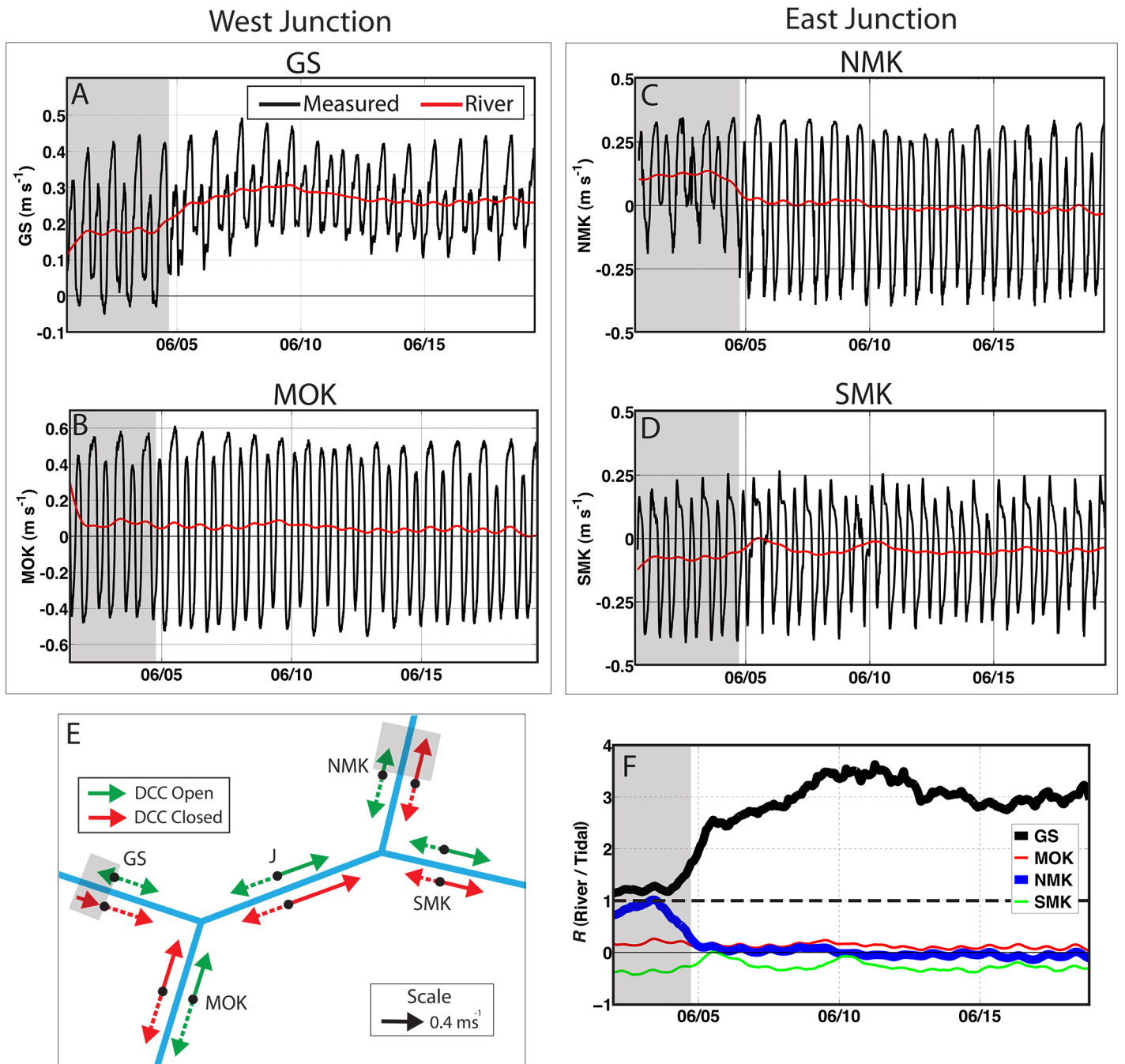
The ratio of the subtidal to tidal velocity,

Figure 6 Comparison of measured and riverine velocities in the west junction at **(A)** GS and **(B)** MOK and in the east junction at **(C)** NMK and **(D)** SMK. Measured velocities are the depth-averaged, instantaneous velocities; the river velocities are the depth-averaged, subtidal velocities found by low-pass filtering the measured velocity with a 25-hr window. **(E)** Peak velocities during flood and ebb tide at each ADCP mooring when the DCC was open (green) and closed (red). **(F)** River to tidal velocity ratio, R, at GS, MOK, NMK, and SMK. The grey box highlights when the DCC was open and the dotted black line shows the river to tidal ratio of 1, which signifies the transition from river to tidal forcing dominance. NMK and GS lines are thicker to emphasize that these two locations reacted the most to the DCC operations.

$$R = \frac{\langle u \rangle}{u_{Trms}}$$

(4)

describes the relative importance of tidal and subtidal (i.e., riverine) currents in the Delta. R indicates the integrated effect of upstream water operations (for example, at the DCC) on water transport downstream; e.g., when $R > 1$, river flow dominates scalar transport. The variability of R will be discussed at each ADCP mooring (Figure 6F).

For SMK, R was generally negative, which reveals that the SMK subtidal flow was upstream, since the tidal constituent, u_{Trms} , was always positive. Additionally, since $R < 1$, tidal currents were stronger than subtidal currents. Nonetheless, mean upstream transport, which was against the river flow during the study period, was expected in SMK, and is supported by drifter and modeling results in the coming sections.

For NMK, subtidal velocities were dominant when the DCC was open ($R > 1$). However, R dropped to 0 when the DCC closed, signifying that transport in NMK was determined by the river flows when the DCC was open and by tides when the DCC was closed. This change in flow ratio is expected because opening the DCC diverts Sacramento-derived flow into NMK, causing NMK to be primarily riverine-influenced. On the other hand, less Sacramento flow was available for GS, resulting in GS riverine velocities dropping to the same magnitude as the tidal velocities and lowering R when the DCC was open. For GS, the value of R implies that tides could affect scalar transport within GS when the DCC was open, even though the mean flow was always downstream. Inversely, river flow in GS, largely from the Sacramento, determined movement of scalars in GS when the DCC was closed. Thus, from an operational standpoint, the riverine to tidal ratio, R, highlights the link between gate operations and scalar transport into and out of junctions in the Delta. Additionally, the subtidal to tidal ratio can help predict particle movement—downstream or upstream with the dominant river or tidal velocity.

Power Spectral Density of Junction Channel Velocities

The power spectral density highlights the most energetic frequencies of motions in the water column. The NMK PSD shows the expected dominance of the diurnal and semi-diurnal frequencies, although the latter was much attenuated when the DCC was open (Figure 7A). When the DCC was closed, the semi-diurnal peak (right dotted line) became 25 times larger (0.0075 to $0.19 \, \mathrm{m^2 \, s^{-2}}$), and the diurnal peak (left dotted line in Figure 7A) was 1.8 times larger (0.017 to $0.03 \, \mathrm{m^2 \, s^{-2}}$). Note that the 95% confidence intervals, which apply to all frequencies in the PSD, do not overlap for NMK, implying that with 95% accuracy the PSDs differ when the DCC was open and closed. In contrast, in the SMK PSD (Figure 7B), the 95% confidence intervals are overlapping, so the DCC open versus closed PSDs are not statistically different with 95% accuracy. When the DCC was closed, the SMK semi-diurnal peak was 2.3 times larger (0.0375 to $0.085 \, \mathrm{m^2 \, s^{-2}}$), and the diurnal peak was 1.6 times larger (0.007 to $0.01 \, \mathrm{m^2 \, s^{-2}}$). While SMK contained more power in the diurnal and semi-diurnal frequencies when the DCC was closed, flow in NMK was most sensitive to the DCC operations. This is consistent with the DCC's enhanced connectivity and closer proximity to NMK relative to SMK, which is further away from the DCC. Thus, the PSD results support that opening the DCC changed NMK from a tidal to riverine environment, which also varied transport in the Delta.

Drifter Results

Drifters provided a Lagrangian view of GSJ, highlighting key flow features in the west and east junctions that affected local mixing (Table 1). We start by presenting a conceptual model of the expected flow features at a convergence, which will serve as a basis for understanding dynamics at the west junction. Next, two drifter paths in the west junction will be discussed, revealing small-scale, intermittent flow features that exist on super-tidal time scales, i.e., time
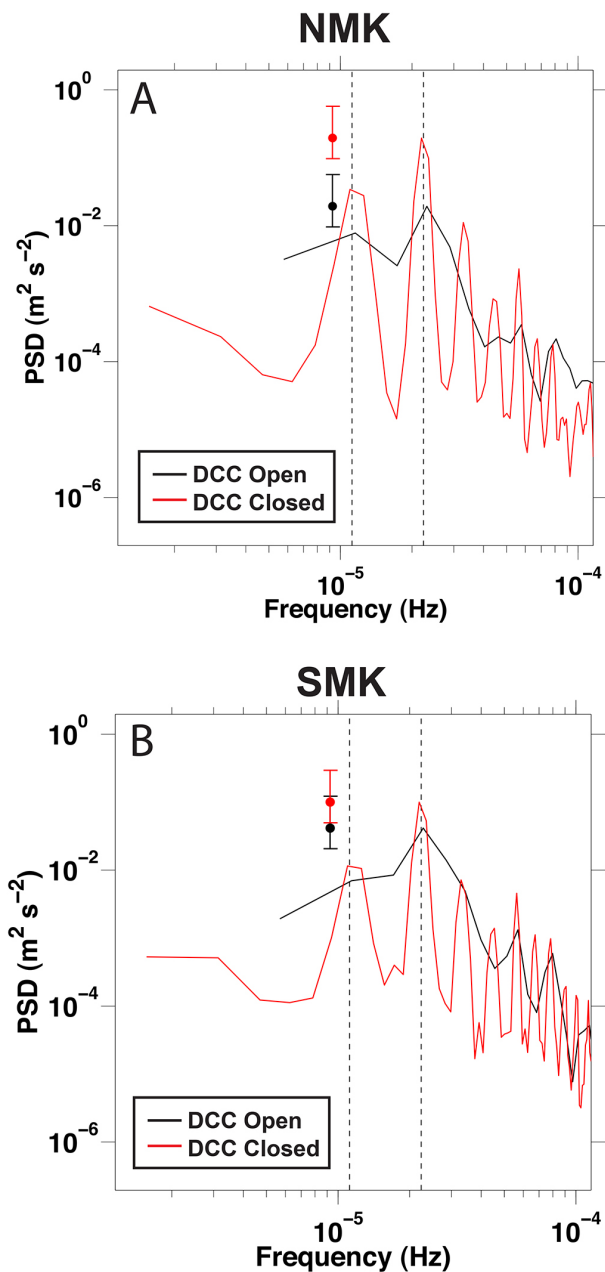
NMK

SMK

Figure 7 The variance preserving power spectral density of NMK **(A)** and SMK **(B)** velocities that were averaged every 10 min and depth averaged. NMK and SMK data were divided into three windows with 50% overlap, de-trended using a linear fit in each sub-window, and multiplied by a Hann window. The black curves denote when the DCC was open (May 31–June 4 at 17:00) and the red when the DCC was closed (June 4 at 17:00 through June 19). The 95% confidence intervals are displayed with the vertical lines with a circle, which apply to all of the frequencies in the PSD. Diurnal and semi-diurnal tidal frequencies are represented by the vertical dotted lines, respectively.

scales smaller than a tidal cycle. Finally, two drifter paths in the east junction will be presented to display that east junction dynamics largely occur on tidal time scales.

Conceptual Model of a Junction

GSJ is composed of the east and west junctions. The east junction behaves as a traditional confluence when downstream flow in NMK and SMK merge; it behaves as a traditional diffluence when flow from the junction diverges into NMK and SMK. The west junction, on the other hand, contains more unique structures because of the scour hole at the corner of the junction, and the tight angle of flow curving around from GS into MOK. A conceptual model for the convergence of the west junction is presented based on literature on junction dynamics (Figure 8) (redrawn to the GSJ from Best and Reid 1984; Weber et al. 2001). Starting in Georgina Slough (GS), water flows downstream to the east into the junction, is diverted sharply to the southwest, and ultimately flows downstream into MOK. A separation zone is expected immediately downstream of the junction channel from flow detaching from the junction head-land. Inside the separation region, a low-pressure zone exists where slow recirculating flow forms. The recirculation zone and a stagnation point directly upstream of the junction contract the outgoing flow, creating a strong jet out of the channel into the junction. Inside the junction, a shear plane with a strong velocity gradient is formed between the merging flows leading to the development of a mixing zone (Best 1987; Best and Roy 1991; Kenworthy and Rhoads 1994; Rhoads and Kenworthy 1995; Weber et al. 2001). It should be noted that the conceptual model displays ebb tide at GSJ and that the features during flood tide, with the exception of the recirculation zone, should be similar but weaker in magnitude because of the smaller angle of convergence.

West Junction: Drifters in Recirculation Zone

A recirculation zone formed at the convergence of GS and the main channel when both branches were flowing downstream, as the junction conceptual model predicted. A group of three drifters on June
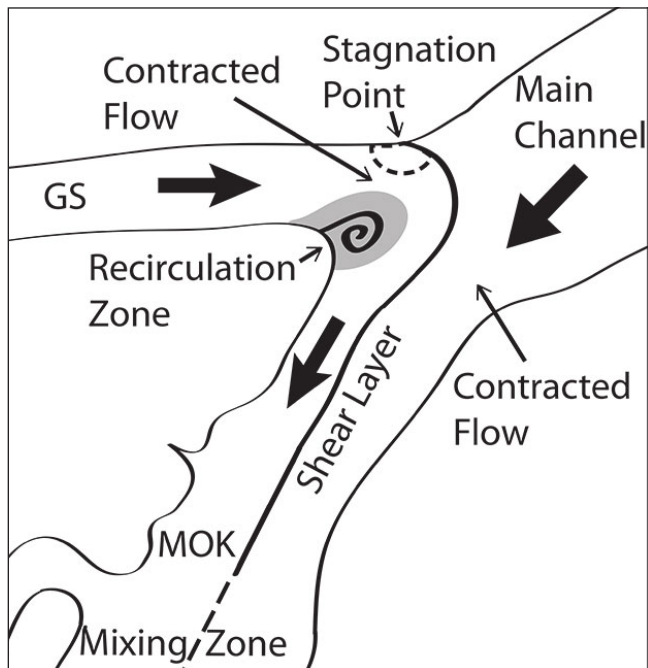
Figure 8 Typical junction characteristics observed at the confluence of Georgiana Slough (GS) flow entering from the west and the main channel flow from the northeast, converging into the Mokelumne (MOK). A recirculation zone forms in the lee of the headland with joined flows from GS and the main channel, mixing along a shear layer. A stagnation point develops at the northern part of the GS flow when it joins the main channel. Redrawn to the GSJ from Best and Reid (1984) and Weber et al. (2001).

8 circled within the eddy with velocities lower than $0.1\,\mathrm{m\,s}^{-1}$ while the six other neighboring drifters traveled directly downstream with velocities near $0.5\,\mathrm{m\,s}^{-1}$ (Figure 9A). SUNTANS streamlines show similar dynamics, including the recirculating eddy (in red) and contraction of streamlines originating in GS and subsequently traversing downstream into MOK. Finally, an ADCP transect over the area where the drifters circled confirms the existence of a recirculation zone (Figure 10). In particular, the small upstream velocities adjacent to the strong downstream velocities in the first half of the transect indicate flow recirculating in the horizontal plane at the corner of GS and MOK. Furthermore, the ADCP transect shows that there was a scour hole at the junction corner with a large change in bathymetry (slope≈0.5), which would enhance the recirculation and increase vertical velocities. Thus, the recirculation zone formed in an energetic part of the junction with strongly heterogeneous flow features.

West Junction: Shear Layer Modification by Large Eddy at West Junction

Two drifter releases in the west junction, one during ebb and the other during flood tide, show that the
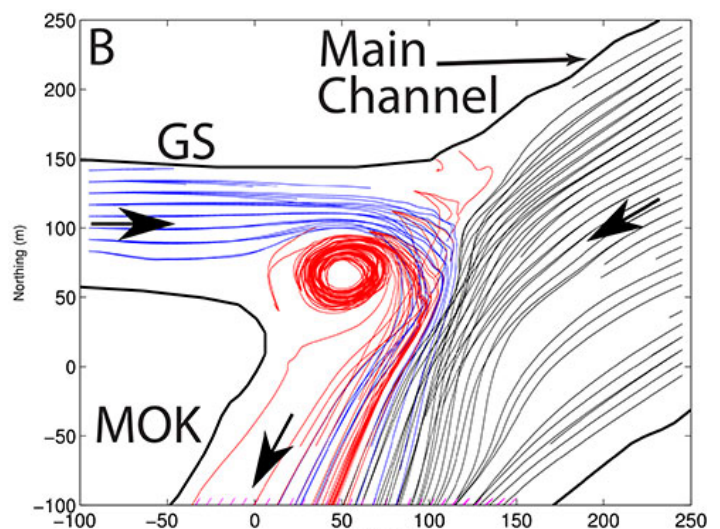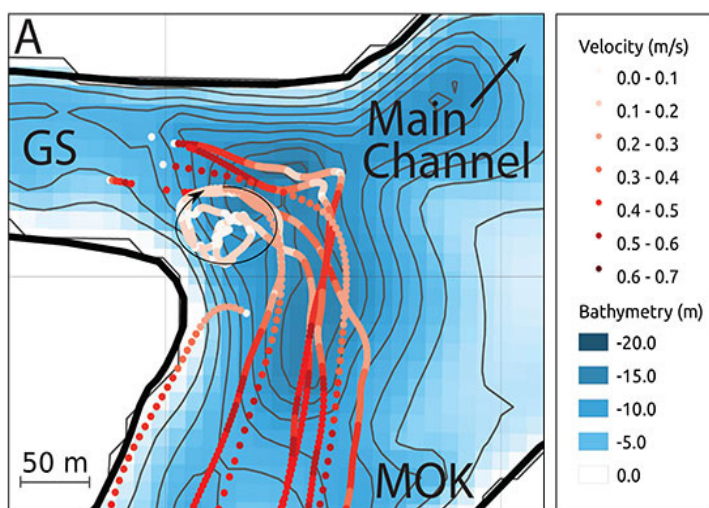

Figure 9 Drifter paths **(A)** and SUNTANS streamlines **(B)** reveal a recirculation zone at the west junction (GS/MOK). **(A)** Group 12 drifter paths on June 8, 2012, from 13:36 to 15:14 during the ebb tide. **(B)** SUNTANS streamlines on May 30, 2012 at 14:00 where red lines denote streamlines originating from the corner region, blue lines originate from GS, and thin black lines originate from the main channel to the northeast of GS.
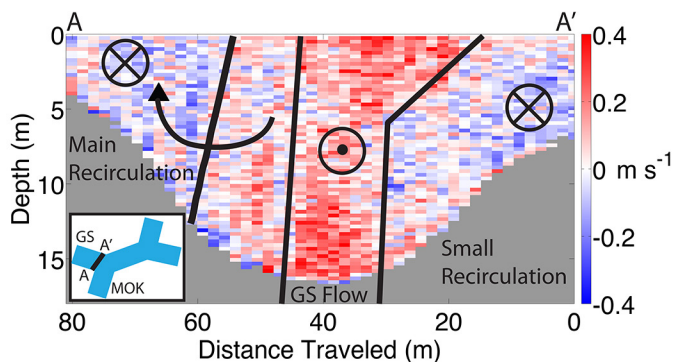
Figure 10 ADCP transecting velocity going from A to A' from 14:39:40 to 14:41:36 on May 30, 2012. This corresponds to MOK and GS on ebb with flow going downstream. Red positive flow represents flow going out of GS (circle with dot): the blue negative flow on the corners of the transect represent flow going upstream into GS (circle with X). Note the large change in bathymetry from the shore to the main channel, equating to a slope of 0.5.

recirculation zone modified the location of the shear layer depending upon ebb or flood tide flow conditions. Drifter paths were asymmetric with respect to ebb and flood tide because the western eddy was transient, forming on ebb tide but disappearing on flood tide. The shear layer, and subsequently drifter paths, compensated for this super-tidal flow feature.

The first drifters (Group 11) were released in NMK and SMK on June 8 during ebb tide when NMK was flowing downstream (Figure 11A). Drifters originating in NMK traveled at speeds over $0.5\,\mathrm{m\,s}^{-1}$ downstream through the junction and moved across the channel, following flow deflected by the presence of the eddy near the corner of GS and MOK. The drifter remained on the eastern side of flow, as delineated by the shear layer shown schematically in Figure 8.

The second drifters (Group 6) were released in MOK on June 1 during flood tide when flow in MOK was upstream. The 10 drifters traveled at approximately $0.4\,\mathrm{m\,s}^{-1}$ upstream and expanded across the cross section in MOK as they approached GS (Figure 12). When the drifters left the MOK stem and entered the main stem (at the black circle), the drifters spread out laterally. Note that although there was some amount of transverse drifter movement along the channel, the
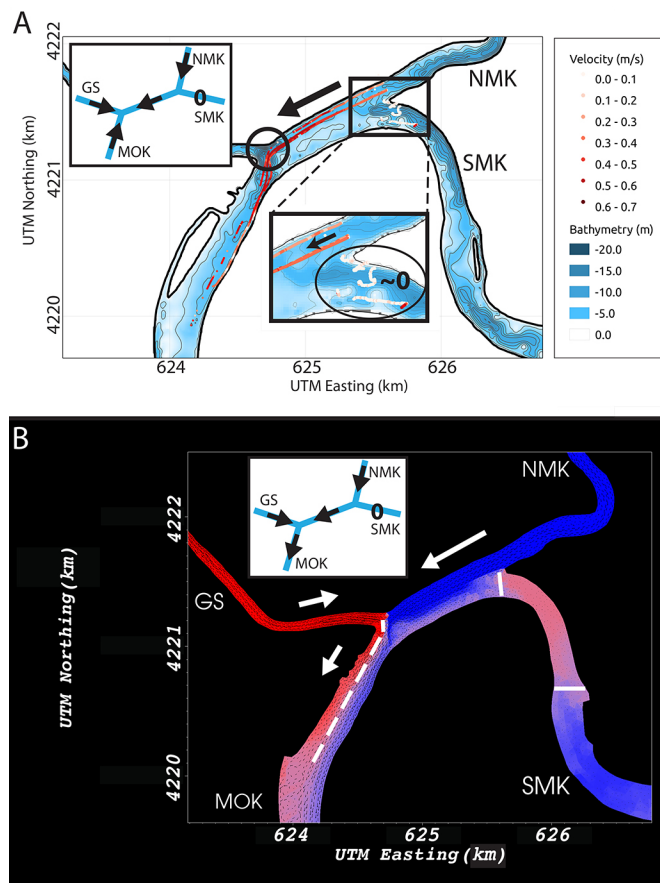

Figure 11 **(A)** Paths of nine drifters released at the entrance of NMK and SMK on June 8, 2012, from 13:25 to 16:56 in Group 11. The intensities of the red color along the path correspond to the drifter velocity and the inset cartoon in the top left of the figure shows mean flow in each branch of GSJ during the drifter run. The other inset displays a close-up perspective of drifters remaining almost stagnant in SMK while moving downstream in NMK. **(B)** SUNTANS simulation on June 1, 2012, at 18:00. While drifters in part **(A)** were deployed on June 8, the NMK and SMK general circulation was similar to the SUNTANS prediction at 18:00 on June 1, where NMK was flowing downstream while SMK was stagnant. Red signifies water that originated from GS and blue represents water from NMK. The white arrows show the flow direction and the dotted white line represents the shear layer between the GS and NMK-derived water. The white lines in SMK show the stagnant patch. The inset cartoons show the mean flow in each branch of Georgia Slough junction during the simulation.

drifters remained in the eastern portion of the channel relative to the shear plane.

East Junction: Phase Lag and Tidal Trapping

Two drifter releases in the east junction indicated that phasing between NMK and SMK velocities created a stagnant, tidally trapped patch of water in SMK. In the first drifter release (Group 1), drifters deployed in NMK during ebb tide on June 1 when the DCC was open made an unexpected (at least *a priori*) U-turn into SMK. Given a downstream, southward flow in NMK, the drifters would be expected to continue downstream towards the MOK station into the main channel then down MOK in the conventional ebb direction. Instead, the drifters turned into SMK (Figure 13). The currents in NMK and SMK were divergent during this period as shown by the depth-averaged velocities highlighted in purple in Figure 14. While NMK was moving downstream (positive velocity), MOK and SMK were traveling upstream (negative velocity). Essentially, slack tide occurred at different times, which created a phase lag and divergent flow between NMK and SMK. The drifter paths reflect these flow phase differences.

During the second release, drifters deployed nearly simultaneously on June 8 in NMK and SMK travelled very different paths (Group 11). While drifters originating in NMK moved at $0.5\,m\,s^{-1}$ downstream, drifters originating in SMK remained nearly stagnant (lower inset in Figure 11A). A form of tidal trapping developed in SMK because flow in NMK continued to be downstream while that in SMK was experiencing slack tide.

SUNTANS Hydrodynamic Modeling Results: Creation of Patches

Hydrodynamic modeling was used to develop the conceptual junction model and interpret the results both from the fixed ADCP stations and the drifter studies. We present six snapshots of a SUNTANS animation representing a 9-hr evolution of tracers originating in GS (red) and NMK (blue) to elucidate the circulation within GSJ over a tidal cycle (Figure 15).
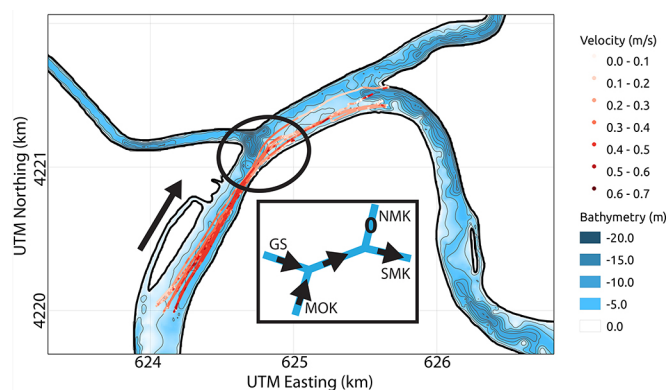

Figure 12 Paths of 10 drifters in Group 6 on June 1, 2012, from 13:10 to 16:17 during flood tide released in MOK and picked up at the entrance of SMK. The circle highlights the shear layer between the GS-derived flow and the mixing zone flow in MOK. The intensities of the red color along the path correspond to the drifter velocity, and the inset cartoon shows the direction of mean flow in each branch of GSJ during the drifter run.
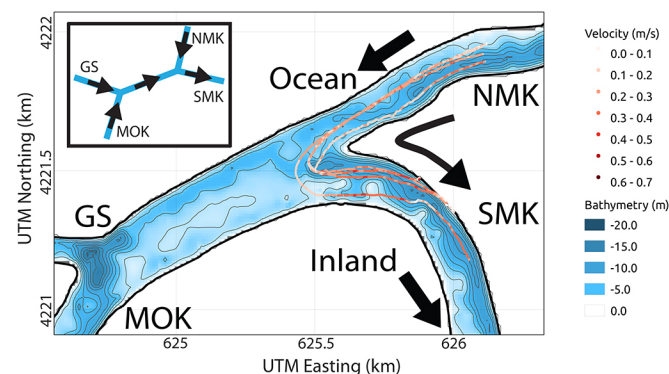

Figure 13 Paths of drifters released in NMK and picked up in SMK on June 1, 2012, from 10:23 to 12:22 in Group 1. The intensities of the red color along the path correspond to the drifter velocity. The inset cartoon shows the mean flow in each branch of GSJ during the drifter run.
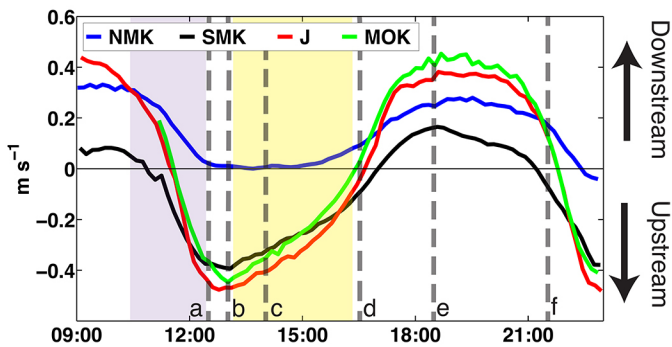
Figure 14 Depth-averaged velocities at four ADCPs on June 1, 2012. Times when the drifters were out in Figure 13 are highlighted in purple and drifters in Figure 12 correspond to the yellow highlighted time. The grey dotted lines marked a, b, c, d, e, and f denote the times that SUNTANS snapshots were taken in Figure 15.

The GSJ circulation can be characterized by the creation of distinct water patches (Figure 15A and 15B), the propagation of the patches upstream in SMK (Figure 15C), and the trapping of a new patch in SMK for approximately half a tidal cycle (Figure 15D–15E) until NMK flow again is directed into SMK (Figure 15F), continuing the cycle as seen in Figure 15A. The flow pattern is curiously reminiscent of that in a beating heart or cycling engine.

The SUNTANS snapshots start on June 1 at 12:30 as the tide propagated up MOK and drove GS flow into the junction (Figure 15A). The upstream-moving GS flow redirected the NMK flow into the SMK, since the NMK had not yet been affected by the tide. Thirty minutes later, the flood tide drove the GS flow to the west junction, cutting off NMK-derived flow within the SMK (Figure 15B). At 14:00, a patch of NMK flow (blue) propagated upstream into SMK as the tide continued to flood MOK and pushed GS-derived flow (red) into the middle of the junction and now into SMK (Figure 15C). Notice that NMK experienced slack tide at both 13:00 and 14:00 (Figure 14, dotted lines at b and c). Two and a half hours later (16:30), a new patch was formed that would be tidally trapped within SMK. Downstream-flowing NMK flow detached the GS-derived flow plug (red) inside of the SMK (Figure 15D). The GS-derived patch remained trapped within SMK as NMK flowed downstream

through the junction with clearly defined shear layers (Figure 15E) until NMK waters flowed into SMK at 21:30 (Figure 15F), approximately 5 hours after the creation of the patch in Figure 15D. After another tidal cycle, water patches would be pumped upstream into the interior Delta to the east since NMK water flows into SMK. Thus, the decoupling between the west and east sections of the junctions drives a patchy, tidal pumping of mixed fluid through the South Mokelumne towards the inner Delta. This patchiness occurs on tidal time scales and the distance between patches scales with the tidal excursion.

DISCUSSION: SYNTHESIS OF ADCP, DRIFTER, AND NUMERICAL RESULTS

The SUNTANS snapshots paired with ADCP and drifter results demonstrate the predominance of GSJ hydrodynamics acting over two distinct time scales, namely super-tidal (i.e., smaller than a tidal cycle), and tidal time scales. The ADCP results in combination with the SUNTANS model results displayed circulation patterns and phasing mechanisms between channel branches that acted primarily over tidal time scales, whereas the drifter results in combination with the SUNTANS model results highlighted mechanisms acting at super-tidal time scales, namely the junction flow features such as a recirculation zone, shear layer, and mixing zone. Below we discuss how these processes affect dispersion within the junction.

How Super-tidal Hydrodynamics Affect Dispersion

The SUNTANS snapshots in Figure 11B and Figure 15 illustrate that flow was not well mixed in GSJ—instead mixing was minimal across shear layers and cohesive patches were distinct throughout the junction. Particularly, the SUNTANS result in Figure 11B shows that a shear layer between NMK and GS (white dotted line) directed and constrained drifters in Figure 11A. Similarly, a mixing zone in Figure 15C restricted drifters to the eastern bank (Figure 12) until they entered a homogeneous source of water (MOK and GS derived), showing that particles within the water were advected by the streamwise currents and were subsequently deflected by flow in the other channels, in this case GS. Thus, the mixing zone and
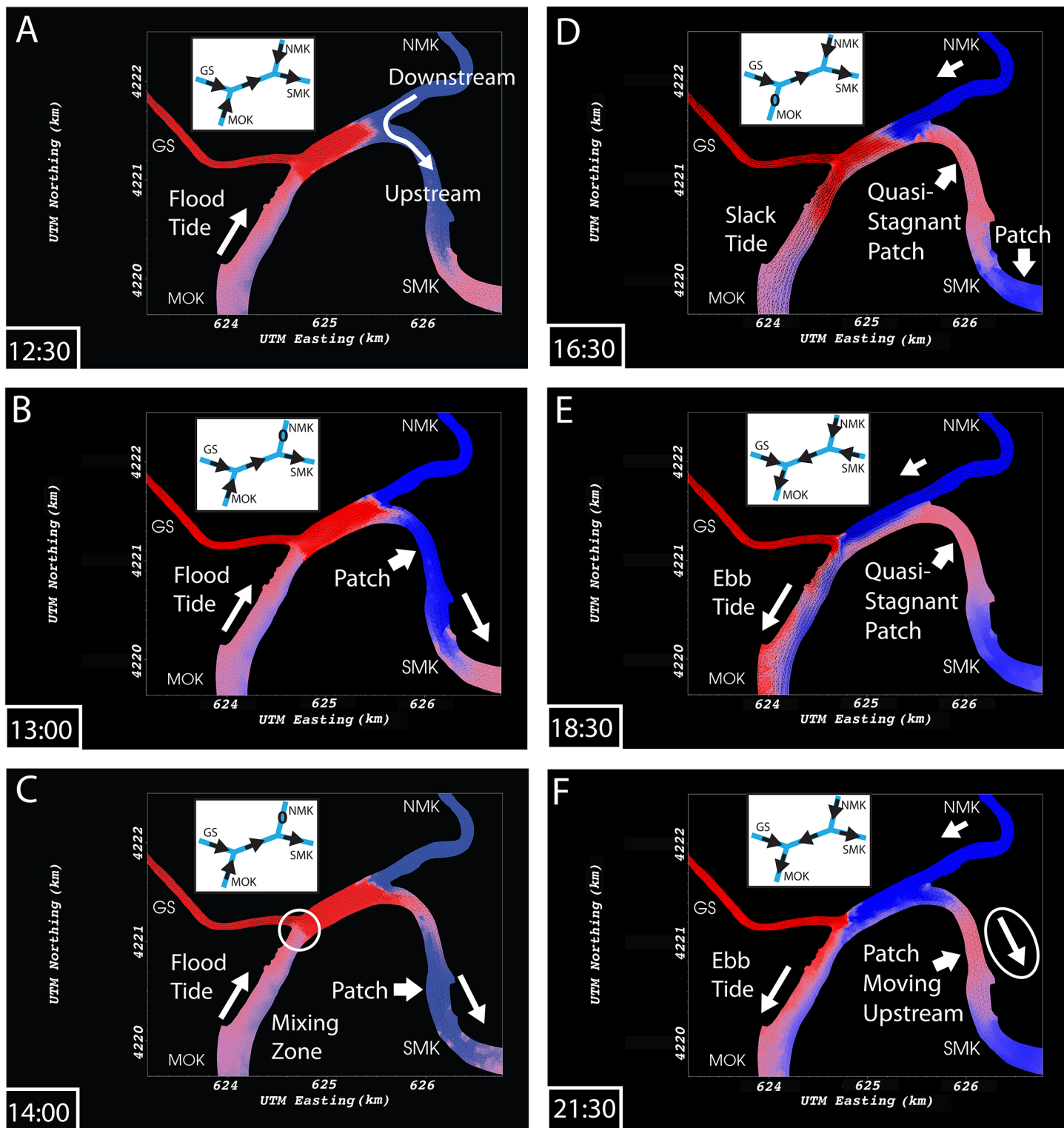
16

Figure 15 SUNTANS simulation for June 1, 2012 at: **(A)** 12:30; **(B)** 13:00; **(C)** 14:00; **(D)** 16:30; **(E)** 18:30 and **(F)** 21:30. Red signifies water that originally came from Georgiana Slough (GS) and blue represents water coming from the North Mokelumne (NMK). The inset cartoons show the mean flow in each branch of GSJ during the simulation.

shear layer inhibited mixing by constricting particles to one side of the channel. We observed that drifters followed the interfaces of junction flow features. This lateral straining of particles effectively changes which branch particles will exit the diffluence. Particle tracking models based on flow-weighted distributions such as DSM2 cannot capture this shear layer dispersion mechanism.

Another feature affecting particle distribution was the recirculation zone at the corner of GS and MOK. This zone enhanced mixing by moving particles laterally (circled in Figure 11A) or trapping particles and separating them in time and space from the initial particle group (Figure 9A). Consequently, the amount of spread between drifters would increase and elevate longitudinal dispersion of ecologically important parameters (Best 1987; Best and Roy 1991; Kenworthy and Rhoads 1994; Rhoads and Kenworthy 1995). Since the recirculation zone varied over time from the phase of the tide and the magnitude of the riverine flow, Wolfram (2014) completed an in depth numerical modeling analysis of intrajunction flow features over many different hydrodynamic conditions. They found that one-dimensional flow-weighted models, such as DSM2, are insufficient to represent junction dynamics because of poor representation of key junction flow features, including the two- and three-dimensional flows at the recirculation zone, the stagnation point, the shear layer, and the mixing zone. Thus, DSM2 cannot account for trapping in the recirculation and stagnation point and will overpredict mixing across the shear layer since complete mixing is assumed within the junction.

Tidal Hydrodynamics

The general circulation can be characterized by advective tidal pumping creating patchiness within the junction. Tidal pumping resulted from the tides affecting the junction branches at different times such that one branch could be flowing downstream while the other was upstream or stagnant. We have defined this phenomenon as phasing between junction channels. Also, this phase lag between branches

entails that slack tide occurred at different times such that distinct water masses were nearly stagnant for several hours. Consequently, phasing differences resulted in tidal trapping and, ultimately, could enhance dispersion.

Tidal Trapping in Junction Channels

Tidal trapping within a junction channel is similar to tidal trapping described by Fischer et al. (1979) where part of a scalar patch such as salt or dye becomes trapped in a side embayment of a river. MacVean and Stacey (2011) extended this diffusive view of trapping to advective forcing, which is more relevant in GSJ. Regardless of the process causing transport into the embayments, these embayments can enhance dispersion because they separate the trapped scalar patch from its original patch until dispersive or advective processes return the patch to the channel. The primary tidal trapping models that have described the dispersion from diffusive and advective tidal traps (Okubo 1973; MacVean and Stacey 2011) may be appropriate for tidal trapping in junction channels.

In GSJ, our results show that tidal trapping enhanced mixing because differences in velocity phasing between junction channels broke up smaller patches of distinct sourced water from its original plume, as illustrated by the patch in SMK in Figure 15. Separation of the original plume into smaller patches was an advective-dominated process occurring over super-tidal time scales that increased the subtidal longitudinal dispersion coefficient. Also, separating the patches enlarged the surface area of the plume and created greater horizontal gradients between patches.

Phase Lag Between NMK and SMK Measured Velocity Components

Flow phasing between junction channels produced a tidal trap in SMK as water in NMK flowed downstream and allowed for transport of scalar patches upstream into the Delta. Periods of flow phasing can be identified at times when NMK and SMK were flowing in opposite directions (i.e., one upstream

while the other was flowing downstream), as in Figure 13. Based on the depth-averaged ADCP velocities, the phasing between NMK and SMK was much more variable when the DCC was open than closed, as displayed by the blue bars representing the standard deviation in Figure 16A. When the gates were open, the phase lag peaked at 7 hours and had a standard deviation of nearly 2 hours, whereas the standard deviation decreased to less than 0.5 hours once the gates closed during our experiment. This phasing indicates that while SMK was influenced by the tide approximately 2 hours before NMK in our study, the two channels were out of phase more often when the DCC was open. The time of flow phasing increased when NMK had greater riverine forcing while simultaneously SMK remained tidally dominated. Hence, the flow offset was a result of different riverine strength between NMK and SMK.

Phase Lag Between NMK and SMK Tidal Velocity Components

While the DCC increased the phasing time between NMK and SMK measured velocities (Figure 16A), it was unclear if the gates had any effect on the tidal constituent of the velocity. The amount of time that the tidal component of NMK and SMK velocities were flowing in opposite directions indicates the phase lag between their ebb tide as well as their flood tide. In Figure 16B, the tidal phase lag when the DCC was open was smaller (mean = 1.15 hrs) and had more variance than when the DCC was closed (mean = 1.5 hrs), indicating that tidal velocities at NMK and SMK were divergent from one another for a longer amount of time when the DCC was closed. When the DCC was open, NMK had a stronger riverine forcing as shown by $R \approx 1$ (Figure 6F) that allowed NMK to flow into SMK (Figure 15A). In particular, NMK flowed downstream into SMK more often when the DCC was open, as indicated by the larger measured velocity phase lag in Figure 16A. NMK had more of an influence on SMK when the DCC was open, so the two channels were more aligned and had a smaller tidal phase lag.

Timing of Slack Tide at NMK

Comparing the stage and velocity at NMK when the DCC was open and closed displays differences in when slack tide (velocity = 0) occurred (Figure 16C and 16D). When the DCC was open, slack tide occurred at erratic times, and some slack tides were skipped. The timing of slack tide also occurred at inconsistent stage heights during the second smaller tide. For example, the slack tide took place closer to the trough of the weaker tide, but on June 2 the slack tide occurred closer to the peak of the weak tide (third red dot). In contrast, when the DCC was closed, the slack tide came at very predictable intervals slightly after the peaks and troughs of the stage. Thus, when the DCC was open, the slack tide took place at maximum flood height and was more irregular in ebb tide height; when the DCC was closed the slack tide occurred slightly after the maximum ebb and flood tide.

CONCLUSIONS

At GSJ, the west and east junctions demonstrated two important hydrodynamic features that can affect transport in the Delta: phasing between flows in channels occurring at tidal time scales and small-scale mixing features such as shear layers and recirculation zones occurring at super-tidal time scales. Phasing at the east junction developed from decoupling of the west and east sections of the junction for short periods of time. This phasing between channels created mixing associated with tidal pumping that, in our modeled flow for the field experiment time period, produced an inland transport in the Delta. At the west junction, small-scale features in the junction such as separation zone eddies, shear layers, and mixing zones serve to either enhance or attenuate longitudinal and transverse mixing depending on the phase of the tide and flow rates.

Ultimately, this experiment shows that phase differences redistribute flows within a junction and cause tidal trapping, creating coherent patches of different water sources within in a junction channel and increasing longitudinal dispersion near the junction and in the Delta. Essentially, junctions can act as
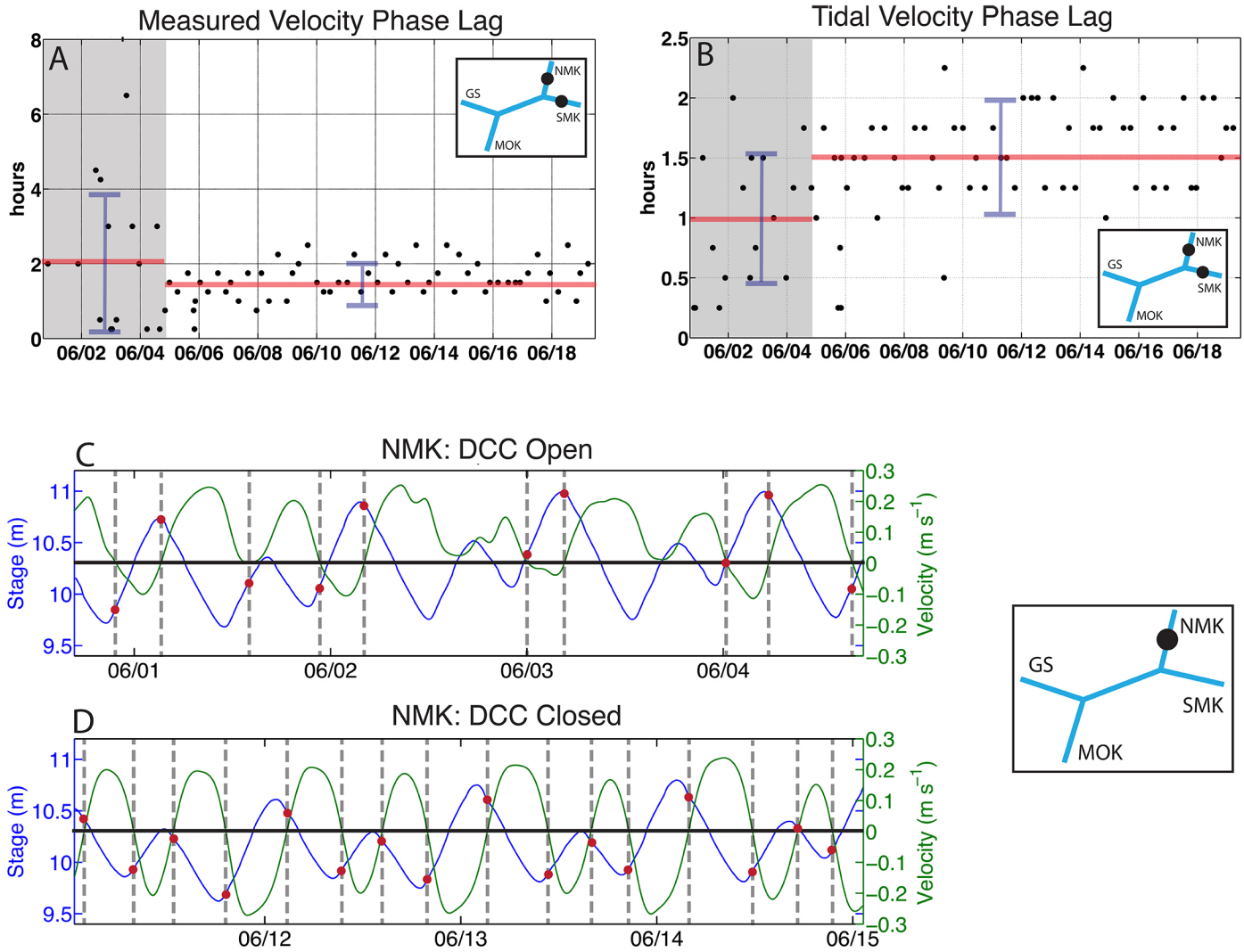
Figure 16 Phase lag between NMK and SMK measured velocities **(A)** and the tidal velocity constituent **(B)**. The grey rectangle highlights when the DCC was open, and the red lines show the average phase lag when the gates were open and closed. Note that the standard deviation is represented by the vertical blue bars. **(C)** A time series of the stage (blue) and velocity (green) at NMK when the DCC was open and when the DCC was closed **(D)**. The grey dotted lines denote when slack tide took place and the red dots correspond to the stage during slack tide.

dispersive mechanisms by relaying scalars down different paths and spreading scalars out in time, which is similar to the tidal trapping in breached ponds described by MacVean and Stacey (2011).

We also found that the timing of slack tide at junction channels is important because it dictates the length of the phase lag between junction branches. Hence, variability in slack tide at junction branches affects the transport of pollutants, nutrients, and fish, and any other material carried by the water. As the phase lag between junction channels increases, as indicated by changes to the timing of slack tide, more scalar patches can be transported upstream into the inner Delta. These patches occur from differences in tidal and riverine influence on junction branches, which can be altered by water management operations. Thus, the extent to which water operations affect transport downstream can be predicted by changes in the riverine to tidal ratio, R.

Specific junction hydrodynamics matter ecologically because they can affect the distribution of phytoplankton, fish and their larvae, sediment, agricultural runoff, and nutrients. Furthermore, future changes to Delta flows, such as modifications to Delta geometry and breaching of levees, will alter the tidal dispersion characteristics of nearby junctions, which in turn will alter environmentally significant characteristics of the Delta. Therefore, there is a great need to understand what dictates the movement of water in the Delta. In response, this paper improves understanding of tidal junction hydrodynamics of the current and future Delta.

ACKNOWLEDGEMENTS

REFERENCES

Allen J, Somerfield P, Gilbert F. 2007. Quantifying uncertainty in high-resolution coupled hydrodynamic-ecosystem models. J Mar Syst [Internet]. [cited 2014 Aug 25];64(1):3–14. Available from: *http://www.sciencedirect.com/science/article/pii/S0924796306001035* doi: *http://dx.doi.org/10.1016/j.jmarsys.2006.02.010*

Best JL, Reid I. 1984. Separation zone at open-channel junctions. J Hydraul Eng-ASCE [Internet]. [cited 2013 Jul 23];110(11):1588–1594. Available from: *http://ascelibrary.org/doi/abs/10.1061/(ASCE)0733-9429(1984)110:11(1588)* doi: *http://dx.doi.org/10.1061/(ASCE)0733-9429(1984)110:11(1588)*

Best JL. 1987. Flow dynamics at river channel confluences: implications for sediment transport and bed morphology. In: Ethridge FG, Flores RM, Harvey MD, editors. Recent developments in fluvial sedimentology. SEPM Special Publication 39. Tulsa (OK): The Society of Economic Paleontologists and Mineralogists p. 27–35.

Best JL, Roy AG. 1991. Mixing-layer distortion at the confluence of channels of different depth. Nature [Internet]. [cited 2013 Jul 25];350:411–13. Available from: *http://www.nature.com/nature/journal/v350/n6317/abs/350411a0.html* doi: *http://dx.doi.org/10.1038/350411a0*

Denton RA. 1993. Accounting for antecedent conditions in seawater intrusion modeling–applications for the San Francisco Bay–Delta. In: Shen HW, Su ST, Wen F, editors. Proceedings of the American Society of Civil Engineers Specialty Conference; 1993 Jul 25–30; San Francisco, California. Hydraul Eng [Internet]. [cited 2013 Jul 25];1:448–453. Available from: *http://www.waterboards.ca.gov/waterrights/water_issues/programs/bay_delta/deltaflow/docs/exhibits/ccwd/spprt_docs/ccwd_denton_1993.pdf*

Feyrer F, Newman K, Nobriga M, Sommer T. 2010. Modeling the effects of future outflow in the abiotic habitat of an imperiled estuarine fish. Estuaries Coasts [Internet]. [cited 2013 Jul 24];34:120–28. Available from: *http://www.water.ca.gov/aes/docs/FeyrerNewmanNobrigaSommer2010.pdf* doi: *http://dx.doi.org/10.1007/s12237-010-9343-9*

Fischer HB, List EJ, Koh RCY, Imberger J, Brooks NH. 1979. Mixing in inland and coastal waters. San Diego (CA): Academic Press, Inc. p. 80-103; 253-256.

Foxgrover A, Smith RE, Jaffe BE. 2003. Suisun Bay and Delta bathymetry. United States Geological Survey [Internet]. [cited 2013 Jul 24]. Available from: *http://sfbay.wr.usugs.gov/sediment/delta*

Fringer OB, Gerritsen M, Street RL. 2006. An unstructured-grid, finite-volume, nonhydrostatic, parallel coastal-ocean simulator. Ocean Model [Internet]. [cited 2013 Jul 20];14:139–278. Available from: *http://web.stanford.edu/~fringer/publications/obf_oceanmodelling_2006_14.pdf* doi: *http://dx.doi.org/10.1016/j.ocemod.2006.03.006*

Geyer WR, Signell RP. 1992. A reassessment of the role of tidal dispersion in estuaries and bays. Estuaries [Internet]. [cited 2013 Jul 24];15(2):97–108. Available from: *http://www.jstor.org/stable/1352684*

Holleman R, Fringer OB, Stacey M. 2013. Numerical diffusion for flow-aligned unstructured grids with application to estuarine modeling. Int J Numer Meth Fl [Internet]. [cited 2013 Jul 23];72:1117–1145. Available from: *http://onlinelibrary.wiley.com/doi/10.1002/fld.3774/pdf* doi: *http://dx.doi.org/10.1002/fld.3774*

Horne JH, Baliunas SL. 1986. A prescription for period analysis of unevenly sampled time series. Astrophys J [Internet]. [cited 2013 Jun 28];302:757–763. Available from: *http://adsabs.harvard.edu/full/1986ApJ...302..757H*

Jassby AD, Kimmerer WJ, Monismith SG, Armor C, Cloern JE, Powell TM, Schubel JR, Vendlinski TJ. 1995. Isohaline position as a habitat indicator for estuarine populations. Ecol Appl [Internet]. [cited 2013 Jul 24];5:272–289. Available from: *http://www.esajournals.org/doi/abs/10.2307/1942069* doi: *http://www.esajournals.org/doi/abs/10.2307/1942069*

Kenworthy ST, Rhoads BL. 1995. Hydrologic control of spatial patterns of suspended sediment concentration at a stream confluence. J Hydrol [Internet]. [cited 2013 Jul 24];168:251–263. Available from: *http://www.sciencedirect.com/science/article/pii/002216949402644Q* doi: *http://dx.doi.org/10.1016/0022-1694(94)02644-Q*

Kimmerer WJ, Nobriga ML. 2008. Investigating particle transport and fate in the Sacramento–San Joaquin delta using a particle transport model. San Franc Estuary Watershed Sci [Internet]. [cited 17 July 2013];6(1). Available from: *http://www.escholarship.org/uc/item/547917gn* doi: *http://dx.doi.org/10.15447/sfews.2008v6iss1art4*

MacVean L, Stacey M. 2011. Estuarine dispersion from tidal trapping: a new analytical framework. Estuaries Coasts [Internet]. [cited 2013 Jul 23];34:45–59. Available from: *http://link.springer.com/article/10.1007%2Fs12237-010-9298-x* doi: *http://dx.doi.org/10.1007/s12237-010-9298-x*

Marechal D. 2004. A soil-based approach to rainfall-runoff modelling in ungauged catchments for England and Wales [dissertation]. [Silsoe (UK)]: Cranfield University.

Monismith SG, Hench JL, Fong DA, Nidzieko NJ, Fleenor WE, Doyle L, Schladow SG. 2009. Thermal variability in a tidal river. Estuaries Coasts [Internet]. [cited 2013 Jul 23];32:100–110. Available from: *http://link.springer.com/article/10.1007%2Fs12237-008-9109-9* doi: *http://dx.doi.org/10.1007/s12237-008-9109-9*

Monsen NE. 2000. A study of sub-tidal transport in Suisun Bay and the Sacramento–San Joaquin Delta, California [dissertation]. [Stanford (CA)]: Stanford University.

Okubo A. 1973. Effect of shoreline irregularities on streamwise dispersion in estuaries and other embayments. Neth J Sea Res [Internet]. [cited 2013 Jul 24];6:213–224. Available from: *http://www.sciencedirect.com/science/article/pii/0077757973900148* doi: *http://dx.doi.org/10.1016/0077-7579(73)90014-8*

Rhoads BL, Kenworthy ST. 1995. Flow structure at an asymmetrical stream confluence. Geomorphology [Internet]. [cited 2013 Jul 24];11(4):273–293. Available from: *http://www.sciencedirect.com/science/article/pii/0169555X94000694* doi: *http://dx.doi.org/10.1016/0169-555X(94)00069-4*

Ridderinkhof H, Zimmerman JTF. 1992. Chaotic stirring in a tidal system. Science [Internet]. [cited 2013 Jul 24];258:1107–1109. Available from: *http://www.sciencemag.org/content/258/5085/1107* doi: *http://dx.doi.org/10.1126/science.258.5085.1107*

Scargle JD. 1982. Studies in astronomical time series analysis. II–statistical aspects of spectral analysis of unevenly spaced data. Astrophys J [Internet]. [cited 2013 Jul 20];263:835–853. Available from: *http://articles.adsabs.harvard.edu/full/1982ApJ...263..835S* doi: *http://dx.doi.org/10.1086/160554*

Taylor GI. 1954. The dispersion of matter in turbulent flow through a pipe. Proc Phys Soc B [Internet]. [cited 2013 Jun 10];223A:446–468. Available from: *http://iopscience.iop.org/0370-1301/67/12/301/pdf/0370-1301_67_12_301.pdf* doi: *http://dx.doi.org/10.1088/0370-1301/67/12/301*

Tinka A, Rafiee M, Bayen A. 2013. Floating sensor networks for river studies. IEEE Syst J [Internet]. [cited 2013 Jul 23];7(1):36–49. Available from: *http://bayen.eecs.berkeley.edu/sites/default/files/journals/06268424.pdf* doi: *http://dx.doi.org/10.1109/JSYST.2012.2204914*

[USBR] U.S. Bureau of Reclamation. 2013. Delta Cross Channel dact sheet. Available from: *http://www.usbr.gove/mp/PA/docs/fact_sheets/Delta_Cross_Channel_Canal.pdf*

Weber LJ, Schumate ED, Mawer N. 2001. Experiments on flow at a 90 open channel junction. J Hydraul Eng [Interent]. [cited 2013 Jul 23];127(5):340–350. Available from: *http://ascelibrary.org/doi/abs/10.1061/%28ASCE%290733-9429%282001%29127%3A5%28340%29* doi: *http://dx.doi.org/10.1061/(ASCE)0733-9429(2001)127:5(340)*

Wolfram PJ. 2014. Secondary flows and dispersion in channel junctions [dissertation]. [Stanford (CA)]: Stanford University.